Control and Cybernetics

vol. **41** (2012) No. 1

Godunov-type algorithms for numerical modeling of solar plasma*

by

Krzysztof Murawski[1] **and Dongwook Lee**[2]

[1] Faculty of Mathematics, Physics and Informatics, UMCS
ul. Radziszewskiego 10, 20-031 Lublin, Poland

[2] The Flash Center for Computational Science, The University of Chicago
5747 S. Ellis, Chicago, IL 60637, USA

Abstract: We discuss numerical methods to solve the Cauchy problem for hyperbolic equations, paying attention to equations which describe physical phenomena in fluid dynamics. We concentrate on Godunov-type methods which adopt Riemann solvers. These methods constitute a formidable task due to complexity of hyperbolic equations. Despite this complexity we show that the Godunov-type methods can be successfully applied to simulate complex systems such as described by equations of magnetohydrodynamics. In particular, we simulate thermal mode in a two-dimensional x-point magnetic field topology that is embedded in a gravitationally stratified solar atmosphere.

Keywords: computer science, modelling, numerical methods, hyperbolic equations.

1. Introduction

As a result of their intrinsic complexity, a lot of physical phenomena are described by mathematical equations, which cannot be solved analytically. So, they require a numerical treatment. The basic idea of computer experiments is to simulate the physical evolution by solving an appropriate set of mathematical equations built on the basis of a physical model. It is typical to develop a mathematical model, like a set of differential equations and then to transform them to a discrete form that can be numerically treated. In this way, numerical simulations rely on initialization of a system and attempt to calculate its subsequent events.

Numerical simulations can be used to study the dynamics of complex systems. The class of Godunov-type methods for solving numerically hyperbolic

*Submitted: August 2011; Accepted: March 2012

conservation laws is often regarded as one of the most successful. Godunov (1959) developed the first-order-accurate upwind scheme among a family of simple discretizations. The original first-order scheme of Godunov (1959) uses the self-similar solution of the Riemann problem with piecewise constant initial data to compute the upwind numerical flux. The Riemann problem for a system of conservation laws is defined as the Cauchy problem with initial conditions consisting of two constant states separated by a discontinuity at the origin. The extension to second order of accuracy in time and space can be carried out, e.g., by using a non-oscillatory piecewise linear reconstruction of data from cell averages. It seems that it was Kolgan (1972) who first proposed to reduce spurious oscillations by applying the so-called principle of minimal values of derivatives, producing in this manner a non-oscillatory Godunov-type scheme of second order spatial accuracy. Later on van Leer (1979) developed Monotone Upstream Scheme for Conservation Laws (MUSCL) in which he included higher-order reconstruction.

Construction of numerical schemes of high-order accuracy for solving non-linear hyperbolic conservation law is usually cumbersome. In designing such schemes one faces at least three major difficulties. One of them concerns the preservation of high accuracy in both space and time for multidimensional problems containing source terms. Another one concerns conservation; this is mandatory in the presence of shock waves. The other very important issue relates to generation of spurious oscillations in the vicinity of large gradients; according to Godunov theorem (Godunov, 1959) these are unavoidable by linear schemes of accuracy greater than one. These oscillations pollute the numerical solution and are thus highly undesirable. To avoid generating spurious oscillations, non-linear solution-adaptive schemes must be constructed.

Recently, Murawski and Lee (2011) reviewed numerical methods. That review was limited to the hydrodynamic case only while numerical methods for magnetohydrodynamic (MHD) equations are the subject of the present paper. Murawski and Lee (2011) presented results of advanced numerical simulations for a complex system with a use of a publicly available code, FLASH. However, their studies were limited to acoustic-gravity waves in the solar atmosphere, which are described by Euler equations. The goal here is to employ the FLASH code to solve numerically non-ideal MHD equations for the complex structure of the solar atmospheric plasma. Some effort went also into understanding numerical methods for solving initial-value problem for hyperbolic equations. Thus, we review theory of linear and nonlinear hyperbolic equations in Section 2. We present a few simple finite-difference schemes for scalar hyperbolic equations in Section 3 and devote the following two sections to present MUSCL-Hancock method. We finalize this draft by a presentation of numerical results for a solar plasma and conclusions.

2. Theory of hyperbolic equations

Here, we consider the simplest conceivable hyperbolic equation which is the advection equation. Later on we discuss the Cauchy and Riemann problems for linear and nonlinear sets of hyperbolic equations. As an example we adopt this theory to MHD equations.

2.1. The advection equation

The advection equation is

$$q_{,t} + \lambda q_{,x} = 0\,, \quad |x| < +\infty\,, \quad 0 \le t < +\infty\,, \tag{1}$$

where λ is the advection speed, $q(x,t)$ is generalized density, and the comma with a following subscript denotes the partial differentiation,

$$q_{,t} = \frac{\partial q}{\partial t}\,, \quad q_{,x} = \frac{\partial q}{\partial x}\,. \tag{2}$$

The symbols t and x are, respectively, time and spatial coordinates.

We define *characteristics* as curves $x = x(t)$ in $x - t$ plane, such as

$$\frac{dx}{dt} = \lambda\,, \quad x(0) = x_0\,. \tag{3}$$

Hence

$$x = x_0 + \lambda t\,, \tag{4}$$

where x_0 is the initial point (Fig. 1).

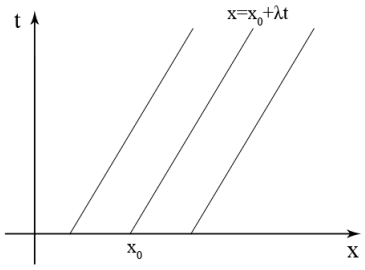

Figure 1. Characteristic curves for the advection equation with $\lambda > 0$.

We evaluate a change of $q(x(t),t)$ along a characteristic curve $x = x(t)$

$$\frac{dq}{dt} = q_{,t} + q_{,x}\frac{dx}{dt} = q_{,t} + \lambda q_{,x} = 0\,. \tag{5}$$

Hence we infer that along $x(t)$ the advection equation becomes the ordinary differential equation and $q(x,t)$ is constant along the characteristic curve.

We consider now *the (Cauchy) initial-value problem* (IVP) for the advection equation,

$$q_{,t} + \lambda q_{,x} = 0\,, \quad |x| < \infty\,,\ t > 0\,, \tag{6}$$

$$q(x, t=0) = q^0(x)\,. \tag{7}$$

To find the solution of the IVP at any point (x,t) we choose the characteristic curve passing through this point and look for the initial point at which the curve crosses the x-axis. As q is constant along $x = x_0 + \lambda t$ we find

$$q(x,t) = q^0(x_0) = q^0(x - \lambda t)\,. \tag{8}$$

The Riemann problem (RP) is the special IVP in which $q(x)$ exhibits a jump at $x = 0$ (Fig. 2), that is

$$q(x,0) = \begin{cases} q_l\,, & x < 0\,, \\ q_r\,, & x \geq 0\,. \end{cases} \tag{9}$$

We find its solution as

$$q(x,0) = q^0(x - \lambda t) = \begin{cases} q_l\,, & x - \lambda t < 0\,, \\ q_r\,, & x - \lambda t \geq 0\,. \end{cases} \tag{10}$$

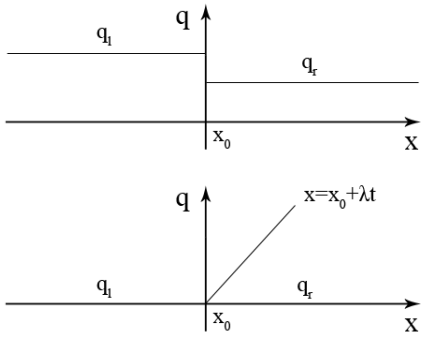

Figure 2. The Riemann problem for the advection equation with $\lambda > 0$.

2.2. System of linear equations

We write a system of linear equations as

$$\mathbf{q}_{,t} + \mathbf{A}\mathbf{q}_{,x} = \mathbf{0}\,. \tag{11}$$

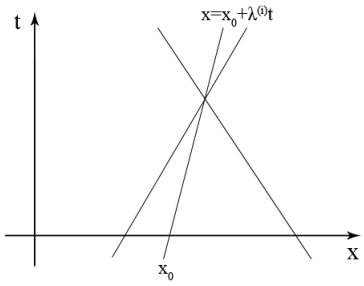

Figure 3. Characteristics of a linear hyperbolic system.

This system is *hyperbolic* if eigenvalues of matrix $\mathbf{A}$ are real and $\mathbf{A}$ has a corresponding complete set of m linearly independent eigenvectors. The system is called strictly hyperbolic if the eigenvalues are all distinct. The eigenvalues of $\mathbf{A}$ are the roots of the characteristic polynomial

$$|\mathbf{A} - \lambda^{(k)}\mathbf{I}| = 0\,, \quad k = 1, \ldots, m\,, \tag{12}$$

where $\mathbf{I}$ the unit matrix. *A right eigenvector* $\mathbf{r}^{(k)}$ of $\mathbf{A}$ is

$$\mathbf{A}\mathbf{r}^{(k)} = \lambda^{(k)}\mathbf{r}^{(k)}\,, \quad k = 1, \ldots, m\,. \tag{13}$$

2.3. The Cauchy problem for a linear system

We specify the IVP for a linear hyperbolic system as

$$\mathbf{q}_{,t} + \mathbf{A}\mathbf{q}_{,x} = \mathbf{0}\,, \quad \mathbf{q}(x, t = 0) = \mathbf{q}^0(x)\,. \tag{14}$$

Here $\mathbf{q}^0(x)$ is the initial condition which we expand as

$$\mathbf{q}^0(x) = \sum_{i=1}^{m} w_i^0(x)\mathbf{r}^{(i)}\,. \tag{15}$$

We write the solution as (LeVeque, 2002)

$$\mathbf{q}(x,t) = \sum_{i=1}^{m} w_i(x,t)\mathbf{r}^{(i)} = \sum_{i=1}^{m} w_i^0(x - \lambda^{(i)}t)\mathbf{r}^{(i)}\,. \tag{16}$$

Hence we infer that at any point (x, t) the solution depends on the initial data at the foots, x_0^i, of m characteristics which cross this point (Fig. 3), $x_0^{(i)} = x - \lambda^{(i)}t\,, \quad i = 1, 2, \ldots, m$. We specify the RP as the IVP for discontinuous

initial data such as

$$\mathbf{q}_{,t} + \mathbf{A}\mathbf{q}_{,x} = \mathbf{0}\,, \tag{17}$$

$$\mathbf{q}(x,0) = \begin{cases} \mathbf{q}_l\,, & x < 0\,, \\ \mathbf{q}_r\,, & x \geq 0\,. \end{cases} \tag{18}$$

With the use of the expansion,

$$\mathbf{q}_l = \sum_{i=1}^{m} \alpha_i \mathbf{r}^{(i)}\,, \quad \mathbf{q}_r = \sum_{i=1}^{m} \beta_i \mathbf{r}^{(i)}\,, \tag{19}$$

we find the solution of this RP in the following form:

$$\mathbf{q}(x,t) = \sum_{i=1}^{i_m} \beta_i(x,t)\mathbf{r}^{(i)} + \sum_{i=i_m+1}^{m} \alpha_i(x,t)\mathbf{r}^{(i)}\,, \tag{20}$$

where for any given point (x,t) we find a maximum i_m of i such that

$$\frac{x}{t} > \lambda^{(i)}\,, \quad i \leq i_m\,. \tag{21}$$

2.4. Nonlinear hyperbolic equations

We start with one-dimensional nonlinear hyperbolic equations,

$$\mathbf{q}_{,t} + \mathbf{f}(\mathbf{q})_{,x} = \mathbf{0}\,. \tag{22}$$

Clearly, the above *differential form* of the conservation law breaks down in the presence of discontinuities such as shocks and contact waves. There are no such drawbacks for the *integral form* of the conservation law, which is

$$\frac{d}{dt}\int_{x_l}^{x_r} \mathbf{q}(x,t)\,dx = \mathbf{f}(\mathbf{q}(x_l,t)) - \mathbf{f}(\mathbf{q}(x_r,t))\,. \tag{23}$$

Here x_l and x_r are chosen arbitrarily. The integral form works for both continuous and discontinuous solutions. For a smooth $\mathbf{q}(x,t)$

$$\int_{x_l}^{x_r} \mathbf{q}(x,t_2)\,dx = \int_{x_l}^{x_r} \mathbf{q}(x,t_1)\,dx + \int_{t_1}^{t_2} \left[\mathbf{f}(\mathbf{q}(x_l,t)) - \mathbf{f}(\mathbf{q}(x_r,t))\right]\,dt\,. \tag{24}$$

The above form is used for construction of finite-volume numerical methods.

Nonlinear hyperbolic equations possess, in particular, shock solutions. A shock moves with speed λ_s, given by the *Rankine-Hugoniot condition* (Toro, 2009)

$$\Delta\mathbf{f} = \lambda_s \Delta\mathbf{q}\,, \tag{25}$$

where

$$\Delta\mathbf{f} = \mathbf{f}(\mathbf{q}_r) - \mathbf{f}(\mathbf{q}_l), \quad \Delta\mathbf{q} = \mathbf{q}_r - \mathbf{q}_l\,. \tag{26}$$

We infer that for $\Delta\mathbf{q}$ corresponding to a shock we get the flux difference, $\Delta\mathbf{f} \sim \Delta\mathbf{q}$. Otherwise, a discontinuity $\Delta\mathbf{q}$ splits into waves. For a linear system $\mathbf{f} = \mathbf{A}\mathbf{q}$ and a shock is admitted for a jump $\Delta\mathbf{q}$ being an eigenvector of $\mathbf{A}$ and λ_s its eigenvalue.

2.4.1. The one-dimensional MHD equations

The MHD equations can be written in the conservative form

$$\mathbf{q}_{,t} + \nabla \cdot \mathbf{f} = 0, \quad \nabla \cdot \mathbf{B} = 0, \tag{27}$$

where:

$$\mathbf{q} = (\varrho, \varrho\mathbf{v}, \mathbf{B}, E)^T, \tag{28}$$

$$\mathbf{f} = (\ \varrho\mathbf{v}, \varrho\mathbf{v}\mathbf{v} + \mathbf{I}(p + \frac{B^2}{2}) - \mathbf{B}\mathbf{B}, \mathbf{v}\mathbf{B} - \mathbf{B}\mathbf{v}, \\ (E + p + \frac{B^2}{2})\mathbf{v} - \mathbf{B}(\mathbf{v} \cdot \mathbf{B})\ )^T. \tag{29}$$

Here $\mathbf{I}$ is the 3×3 identity matrix, $\mathbf{v}\mathbf{v}$ stands for the 3×3 tensor $v_i v_j$, $\mathbf{B}$ has been normalized by $\sqrt{\mu}$, and ^{T} corresponds to a transposed vector.

We rewrite the momentum equation from equation (27) as follows:

$$(\varrho\mathbf{v})_{,t} + \nabla \cdot (\varrho\mathbf{v}\mathbf{v}) + \nabla(p + \frac{B^2}{2}) - (\mathbf{B} \cdot \nabla)\mathbf{B} - \mathbf{B}(\nabla \cdot \mathbf{B}) = 0. \tag{30}$$

The last term of this equation should be equal to zero. If nevertheless $\nabla \cdot \mathbf{B}$ differs from zero, it becomes an additional unphysical force, parallel to $\mathbf{B}$. It has a destabilizing effect on numerical algorithms. Brackbill and Barnes (1980) noted that this instability can be removed by adding $-\mathbf{B}(\nabla \cdot \mathbf{B})$ to the right hand side of Eq. (30). This procedure leads to a non-conservative form of the MHD equations.

One of the most popular approaches to write the MHD equations in the non-conservative form is due to Powell (1994)

$$\mathbf{q}_{,t} + \nabla \cdot \mathbf{f} = -\nabla \cdot \mathbf{B}(0, \mathbf{B}, \mathbf{v}, \mathbf{v} \cdot \mathbf{B})^T, \quad \nabla \cdot \mathbf{B} = 0. \tag{31}$$

It is interesting to check how this change affects the induction equation which can be now written as

$$\mathbf{B}_{,t} + \mathbf{v}(\nabla \cdot \mathbf{B}) + \mathbf{B}(\nabla \cdot \mathbf{v}) - (\mathbf{B} \cdot \nabla)\mathbf{v} = 0. \tag{32}$$

Taking the divergence of both sides and using the mass continuity equation, we obtain an advection equation for the quantity $\nabla \cdot \mathbf{B}/\varrho$, *i. e.*

$$\left(\frac{\nabla \cdot \mathbf{B}}{\varrho}\right)_{,t} + \mathbf{v} \cdot \nabla \left(\frac{\nabla \cdot \mathbf{B}}{\varrho}\right) = 0. \tag{33}$$

Thus, we have introduced a new *divergence wave* propagating with the speed $\mathbf{v}$. So, a partially conservative form of the multi-dimensional equations, obtained by adding terms proportional to $\nabla \cdot \mathbf{B}$, retains the one-dimensional eigenvalue

problem, with the addition of an eighth wave convecting $\nabla \cdot \mathbf{B}$ as a passive scalar.

Alternatively, the MHD equations can be written in the conservative form that also preserves the solenoidal constraint numerically. We consider a method called "constrained transport (CT)" approach which maintains the constraint by solving the induction equation on a staggered grid (Evans and Hawley, 1988; Balsara and Spicer, 1999). A CT based, solution accurate and efficient multidimenional MHD scheme (Lee and Deane, 2009) has been extended from the corner transport upwind algorithm (Colella, 1990). The method keeps the divergence-free constraint by using a CT staggered-grid which places the magnetic field components at the centroids of appropriate cell faces and volumetric variables such as mass, momentum and energy are stored at the centroids of computational cells. On such grid the MHD equations can be approximated in a way that preserves selenoidality of discrete magnetic field. We use this method for the results presented in this paper.

The original MHD equations can be written in the quasilinear form

$$\bar{\mathbf{q}}_{,t} + \mathbf{A}\bar{\mathbf{q}}_{,x} = \mathbf{0}, \tag{34}$$

where the state vector, $\mathbf{q}$, is

$$\bar{\mathbf{q}} = (\ \varrho(x), \varrho(x)\mathbf{v}(x), \mathbf{B}(x), p(x)\ )^T \tag{35}$$

and (Powell, 1994)

$$\mathbf{A} = \begin{pmatrix} v_x & \varrho & 0 & 0 & 0 & 0 & 0 & 0 \\ 0 & v_x & 0 & 0 & -\frac{B_x}{\varrho} & \frac{B_y}{\varrho} & \frac{B_z}{\varrho} & \frac{1}{\varrho} \\ 0 & 0 & v_x & 0 & -\frac{B_y}{\varrho} & -\frac{B_x}{\varrho} & 0 & 0 \\ 0 & 0 & 0 & v_x & -\frac{B_z}{\varrho} & 0 & -\frac{B_x}{\varrho} & 0 \\ 0 & 0 & 0 & 0 & 0 & 0 & 0 & 0 \\ 0 & B_y & -B_x & 0 & -v_y & v_x & 0 & 0 \\ 0 & B_z & 0 & -B_x & -v_z & 0 & v_x & 0 \\ 0 & \gamma p & 0 & 0 & (\gamma-1)\mathbf{v}\cdot\mathbf{B} & 0 & 0 & v_x \end{pmatrix}. \tag{36}$$

It is noteworthy that the 5-th row of matrix $\mathbf{A}$ consists of zeros. This is a consequence of the fact that $(\nabla \cdot \mathbf{B})_{,t} = 0$. As a result, the 8-th eigenvalue of $\mathbf{A}$ is zero, which is unphysical. A remedy is to rewrite Eq. (31) in the quasilinear form

$$\bar{\mathbf{q}}_{,t} + \bar{\mathbf{A}}\bar{\mathbf{q}}_{,x} = \mathbf{0}, \tag{37}$$

where:

$$\bar{\mathbf{A}} = \begin{pmatrix} v_x & \varrho & 0 & 0 & 0 & 0 & 0 & 0 \\ 0 & v_x & 0 & 0 & 0 & \frac{B_y}{\varrho} & \frac{B_z}{\varrho} & \frac{1}{\varrho} \\ 0 & 0 & v_x & 0 & 0 & -\frac{B_x}{\varrho} & 0 & 0 \\ 0 & 0 & 0 & v_x & 0 & 0 & -\frac{B_x}{\varrho} & 0 \\ 0 & 0 & 0 & 0 & v_x & 0 & 0 & 0 \\ 0 & B_y & -B_x & 0 & 0 & v_x & 0 & 0 \\ 0 & B_z & 0 & -B_x & 0 & 0 & v_x & 0 \\ 0 & \gamma p & 0 & 0 & 0 & 0 & 0 & v_x \end{pmatrix}. \tag{38}$$

So, we see that the zero row has disappeared and the eight wave now satisfies the advection equation

$$w^8{}_{,t} + v_x w^8{}_{,x} = 0. \tag{39}$$

As this wave carries non-zero magnetic field divergence it is nicknamed the *divergence* wave.

The Jacobian matrix $\bar{\mathbf{A}}$ has the eigenvalues (λ) and left ($\mathbf{l}$) and right ($\mathbf{r}$) eigenvectors which correspond to four magnetoacoustic waves, two Alfvén waves, one entropy wave, and one divergence wave (Powell, 1994). The Alfvén and magnetoacoustic eigenvectors become singular under certain conditions but these singularities are well treated (Powell, 1994).

We conclude by saying that the RP is solved by the jumps (simple waves) which separate constant states. These jumps are proportional to rigth eigenvectors, $\mathbf{r}^{(i)}$, of the matrix $\mathbf{A}$ and they travel with characteristic speeds $\lambda^{(i)}$. Here $\mathbf{A}\mathbf{r}^{(i)} = \lambda^{(i)}\mathbf{r}^{(i)}$, $i = 1, 2, \ldots, m$.

3. Finite-difference schemes for scalar hyperbolic equations

We present and discuss here finite-difference and finite-volume schemes for scalar hyperbolic equations. We evaluate numerical errors, derive stability conditions, and present the approximate Roe solver.

3.1. Godunov scheme for the advection equation

We approximate partial derivatives with finite-differences; for the temporal and spatial derivatives we adopt, respectively, the *forward* and *backward Euler schemes*:

$$q_{,t} = \frac{q_i^{n+1} - q_i^n}{\Delta t}, \quad q_{,x} = \frac{q_i^n - q_{i-1}^n}{\Delta x}, \tag{40}$$

where

$$q_i^n = q(x_i, t^n) \tag{41}$$

and a grid size Δx and a time-step Δt are

$$x_i = i\Delta x\,, \quad i = 0, 1, \ldots, i_{max}\,, \quad \Delta x = x_{i+1} - x_i\,, \tag{42}$$

$$t^n = n\Delta t\,, \quad n = 0, 1, \ldots, n_{max}\,, \quad \Delta t = t^{n+1} - t^n\,. \tag{43}$$

Substituting these schemes into the advection equation of Eq. (1), we get the *upwind (Godunov) scheme* (Godunov, 1959)

$$q_i^{n+1} = q_i^n + c(q_{i-1}^n - q_i^n)\,. \tag{44}$$

As a result, updating the solution in each numerical cell requires two states.

$$q_i^{n+1} = q_i^n + c(q_{i-1}^n - q_i^n)\,, \tag{45}$$

where c is the Courant-Friedrichs-Lewy (CFL or Courant) number,

$$c = \frac{\lambda\Delta t}{\Delta x} = \frac{\lambda}{\Delta x/\Delta t} = \frac{\text{advection speed}}{\text{grid speed}}\,. \tag{46}$$

Hence, we compute explicitly the evolution of q in time at every i-point, except for $i = 0$. At this point we need to specify boundary conditions. As an example we present transmissive boundary condition as

$$q_0^n = q_1^n\,. \tag{47}$$

3.2. Local truncation error and a modified equation

We replace in the upwind scheme q_i^n by the exact solution, $q(x,t)$, of the advection equation, evaluated at (x_i, t^n). Thus, we arrive at

$$L(q(x_i,t^n)) = \frac{q(x_i,t^{n+1}) - q(x_i,t^n)}{\Delta t} + \quad \lambda\frac{q(x_i,t^n) - q(x_{i-1},t^n)}{\Delta x}\,. \tag{48}$$

For a smooth $q(x,t)$ we adopt Taylor's expansion and get *local truncation error*

$$L_{TE} = \left[\frac{\lambda\Delta x}{2}(c-1)q_{,xx} + \mathcal{O}((\Delta t)^2) + \mathcal{O}((\Delta x)^2)\right]_i^n\,. \tag{49}$$

We infer that the upwind scheme is first-order accurate in space, see also LeVeque (2002). Note that $q(x,t)$ does not satisfy the advection equation (1) but, instead, the *modified equation* in which $q_{,xx}$ corresponds to diffusion.

3.3. The von Neumann stability analysis

A numerical scheme is unstable if numerical errors grow in time. On the other hand, stability relies on controlling spurious oscillations. Stability of a numerical scheme can be analyzed by the von Neumann method (von Neumann and Richtmeyer, 1950). In this method we consider a plane wave

$$q_i^n = A^n e^{Ii\theta}\,. \tag{50}$$

Here θ is a phase and $I = \sqrt{-1}$ is the imaginary unit. Substituting Eq. (50) into the upwind scheme, we get *the amplification factor*

$$|A| = \sqrt{(1-c)^2 + c^2 + 2c(1-c)\cos\theta}\,. \tag{51}$$

The stability condition $|A| \le 1$ implies $0 \le c \le 1$. Hence the time step is constrained as $\Delta t \le \frac{\Delta x}{\lambda}$. In practice we introduce the Courant number $c_{cfl} = \lambda\Delta t/\Delta x$. Then

$$\Delta t = c_{cfl}\frac{\Delta x}{\lambda}\,, \quad 0 < c_{cfl} \le 1\,. \tag{52}$$

For safety reasons it is recommended to use $0 < c_{cfl} < 1$, e.g. $c_{cfl} = 0.8$.

3.4. Finite-volume methods for a system of equations

We discretize the system of one-dimensional hyperbolic equations with the use of *finite-volume method* which stands as

$$\mathbf{q}_i^{n+1} = \mathbf{q}_i^n + \frac{\Delta t}{\Delta x}(\mathbf{f}_{i-1/2} - \mathbf{f}_{i+1/2})\,. \tag{53}$$

Here we implemented cell averaged $\mathbf{q}_i^n$ and time-averaged $\mathbf{f}_{i\pm1/2}^n$ as

$$\mathbf{q}_i^n = \frac{1}{\Delta x}\int_{x_{i-1/2}}^{x_{i+1/2}} \mathbf{q}(x,t^n)\,dx\,, \quad \mathbf{f}_{i+1/2}^n = \frac{1}{\Delta t}\int_t^{t+\Delta t} \mathbf{f}(\mathbf{q}(x_{i+1/2},t))\,dt\,. \tag{54}$$

A key issue is to compute a numerical flux $\mathbf{f}_{i+1/2}^n$. One way of evaluating $\mathbf{f}_{i+1/2}^n$ is to adopt the averaging

$$\mathbf{f}_{i\pm1/2}^n = \frac{1}{2}(\mathbf{f}_i^n + \mathbf{f}_{i\pm1}^n)\,, \tag{55}$$

which is ineffective and may lead to instabilities. An adequate way is given below.

3.5. The Roe solver

For small jumps in the RP, it suffices to use an approximate Riemann solver, based on a local replacement of the nonlinear equations by a linear hyperbolic system like

$$\mathbf{q}_{,t} + \mathbf{A}(\bar{\mathbf{q}})\mathbf{q}_{,x} = \mathbf{q}_{,t} + \bar{\mathbf{A}}(\mathbf{q}_l,\mathbf{q}_r)\mathbf{q}_{,x} = \mathbf{0}. \tag{56}$$

This idea was coined by Roe (1981) who introduced an average Jacobian matrix $\bar{\mathbf{A}}(\mathbf{q}_l,\mathbf{q}_r)$, approximating the Jacobian matrix, $\mathbf{A}(\bar{\mathbf{q}}) = \mathbf{f}_{,\mathbf{q}}(\bar{\mathbf{q}})$. Here $\mathbf{q}_l$ and $\mathbf{q}_r$ are respectively the left and right states in the Riemann problem. The average Jacobian (called also the Roe matrix) is such that for any given left and right pair of states $(\mathbf{q}_l,\mathbf{q}_r)$ the so-called Property U is satisfied:

(i) $\bar{\mathbf{A}}(\mathbf{q}_l, \mathbf{q}_r)$ is a linear mapping from the vector space containing a vector $\mathbf{q}$ to the vector space containing a flux $\mathbf{f}$;
(ii) $\bar{\mathbf{A}}(\mathbf{q}_l, \mathbf{q}_r) \to \mathbf{f}_{,\mathbf{q}}$ as $\mathbf{q}_l$ and $\mathbf{q}_r \to \mathbf{q}$;
(iii) $\bar{\mathbf{A}}(\mathbf{q}_l, \mathbf{q}_r)$ has real eigenvalues and a complete set of linearly independent eigenvectors;
(iv) $\bar{\mathbf{A}}(\mathbf{q}_r - \mathbf{q}_l) = \mathbf{f}_r - \mathbf{f}_l$ for any $\mathbf{q}_l$ and $\mathbf{q}_r$.

The average state $\bar{\mathbf{q}}$ is taken so that property (iv) is satisfied. In the case of the MHD equations, the average mass density is given by $\bar{\varrho} = \sqrt{\varrho_l \varrho_r}$, and the remnant variables such as $\mathbf{V}$, $\mathbf{B}$, E, denoted here by ϕ, are averaged as

$$\bar{\phi} = \frac{\sqrt{\varrho_l}\phi_l + \sqrt{\varrho_r}\phi_r}{\sqrt{\varrho_l} + \sqrt{\varrho_r}}. \tag{57}$$

Once all the averaged variables are obtained, the linearized RP for (56) is considered at each interface. The exact solution of this approximate problem can be expressed in terms of right eigenvector $\mathbf{r}^{(i)}$ of $\bar{\mathbf{A}}$ as

$$\Delta\mathbf{q} \equiv \mathbf{q}_r - \mathbf{q}_l = \sum_{i=1}^{m} \alpha^{(i)} \mathbf{r}^{(i)}. \tag{58}$$

According to property (iv), using(58), we get the vector flux increment expressed as a product of $\Delta\mathbf{q}$ and the corresponding eigenvalue $\lambda^{(j)}$, viz.

$$\Delta\mathbf{f} = \mathbf{f}_r - \mathbf{f}_l = \sum_{j=1}^{m} \alpha^{(j)} \lambda^{(j)} \mathbf{r}^{(j)}\,. \tag{59}$$

The intercell flux can be expressed as

$$\mathbf{f}_{i+1/2} = \frac{1}{2}\left[\mathbf{f}_l + \mathbf{f}_r - \sum_{i=1}^{m} \alpha^{(j)} |\lambda^{(j)}| \mathbf{r}^{(j)}\right]. \tag{60}$$

We conclude this part by saying that high-resolution schemes should be at least second-order accurate in smooth regions of the solution, free from spurious oscillations, and give high-resolution of discontinuities. Therefore, we have to circumvent Godunov (1959) theorem by constructing nonlinear schemes which are discussed next.

4. Higher-order numerical schemes for hyperbolic equations

The low accuracy and the complexity of the Godunov method meant that other methods needed to be developed. Such development effort was undertaken by Kolgan (1972) who proposed to suppress spurious oscillations and produced a non-oscillatory Godunov-type scheme of second-order spatial accuracy. Further, more well-known, developments were due to van Leer (1979) who extended

Godunov approach to second-order spatial accuracy by the MUSCL approach. His approach consists of two key steps: (a) an interpolation (projection or reconstruction) step where, within each cell, the data is approximated by linear functions and (b) an upwind step where the average fluxes at each interface are evaluated by taking into account the wind direction. At step (a) the accuracy was increased by constructing a piecewise linear approximation of $\mathbf{q}(x,t)$ at the beginning of each time-step, viz.

$$\bar{\mathbf{q}}(x,t) = \mathbf{q}_i + \mathbf{s}_i(x - x_i), \quad x_{i-1/2} < x < x_{i+1/2}\,. \tag{61}$$

Here, $\mathbf{s}_i$ is a slope and x_i is the center of the grid cell. So, $\mathbf{q}(x_i,t) = \mathbf{q}_i$. The slope $\mathbf{s}_i$ can be constructed as respectively upwind, downwind, and centered:

$$\mathbf{s}_i = \frac{\mathbf{q}_i - \mathbf{q}_{i-1}}{\Delta x}\,, \quad \mathbf{s}_i = \frac{\mathbf{q}_{i+1} - \mathbf{q}_i}{\Delta x}\,, \quad \mathbf{s}_i = \frac{\mathbf{q}_{i+1} - \mathbf{q}_{i-1}}{2\Delta x}\,. \tag{62}$$

These upwind, downwind and centered slopes lead, respectively, to Beam-Warming, Lax-Wendroff, and Fromm schemes (LeVeque, 2002). Other possibilities include

$$\mathbf{s}_i = minmod(\frac{\mathbf{q}_i - \mathbf{q}_{i-1}}{\Delta x}, \frac{\mathbf{q}_{i+1} - \mathbf{q}_i}{\Delta x})\,. \tag{63}$$

Here the minmod function,

$$minmod(a,b) = \begin{cases} a, & \text{for } |a| < |b| \text{ and } ab > 0\ , \\ b, & \text{for } |a| > |b| \text{ and } ab > 0\ , \\ 0, & \text{for } ab \le 0\ , \end{cases} \tag{64}$$

returns the smallest argument in magnitude if the arguments are of the same sign, and zero if they are not.

Note that choosing $\mathbf{s}_i = 0$ in the above expressions leads to Godunov (1959) method.

4.1. MUSCL-Hancock scheme

As the original MUSCL method (van Leer, 1979) was modified in 1980 by UC Berkeley graduate student of fluid mechanics, Steve Hancock, the modified scheme bears a common name MUSCL-Hancock method. The method consists of the following steps:

1. *Data reconstruction and boundary extrapolated values.* At this stage we reconstruct linear subcell distributions of conservative ($\mathbf{q}_i$) or non-conservative ($\mathbf{w}_i$) vector states and compute intercell values from
$$\mathbf{q}_{il} = \mathbf{q}_i - \frac{1}{2}\Delta x\,\mathbf{s}_i\,, \quad \mathbf{q}_{ir} = \mathbf{q}_i + \frac{1}{2}\Delta x\,\mathbf{s}_i\,. \tag{65}$$
Here $\mathbf{q}_{il}$ ($\mathbf{q}_{ir}$) denotes $\mathbf{q}$ at the left (right) intercell of the i-th grid, $\mathbf{s}_i$ is a limited slope which is introduced in Eq. (61);

2. *Evolution of the boundary values.* The boundary extrapolated values are evolved by a time $\frac{1}{2}\Delta t$ according to
$$\bar{\mathbf{q}}_{il} = \mathbf{q}_{il} + \frac{\Delta t}{2\Delta x}[\mathbf{f}(\mathbf{q}_{il}) - \mathbf{f}(\mathbf{q}_{ir})]\,, \tag{66}$$
$$\bar{\mathbf{q}}_{ir} = \mathbf{q}_{ir} + \frac{\Delta t}{2\Delta x}[\mathbf{f}(\mathbf{q}_{il}) - \mathbf{f}(\mathbf{q}_{ir})]\,. \tag{67}$$
3. *Solution of the RP* for the data
$$\mathbf{q}_i^{l*} = \bar{\mathbf{q}}_{ir}\,, \quad \mathbf{q}_i^{r*} = \bar{\mathbf{q}}_{(i+1)l}\,. \tag{68}$$
Hence we compute the intercell flux $\mathbf{f}_{i+1/2}(\mathbf{q}_i^{l*}, \mathbf{q}_i^{r*})$ with a use of the similarity solution $\mathbf{q}_{i+1/2}(x/t)$
$$\mathbf{f}_{i+1/2} = \mathbf{f}(\mathbf{w}_{i+1/2}(0))\,. \tag{69}$$

Having specified fluxes we can evaluate $\mathbf{q}_{\rm i}^{n+1}$ from the finite-volume scheme of Eq. (53).

5. Application of a Godunov-type method for numerical simulations of thermal mode at the magnetic x-point in the solar atmosphere

Observational findings made by solar missions (e.g., TRACE/EUV, STEREO, SDO) revealed that in the coronal plasma sudden energy release processes take place. These processes can be well described in the framework of solar flares (Aschwanden and Alexander, 2001). We aim to study influence of thermal conduction on attenuation of thermal mode in a gravitationally stratified solar coronal x-point magnetic field topology. Our goal also is to extend the models of De Moortel and Hood (2003), in which damping of slow waves by thermal conduction was studied in the frame of a one-dimensional homogeneous case, and of McLaughlin et al. (2011) who discussed magnetohydrodynamic (MHD) waves in the x-point magnetic field topology. We pay attention to the thermal mode which can be efficiently excited by a gas pressure pulse. As such a pressure pulse can model a sudden energy release, which takes place in a solar flare, we adopt the x-point magnetic field topology which can be present in such flares.

5.1. The numerical model

We perform numerical simulations in a magnetically structured atmosphere. Henceforth, we neglect radiation and plasma heating, viscosity and resistivity but take into account thermal conduction. As a consequence of that we use the following two-dimensional magnetohydrodynamic equations to describe solar plasma:
$$\frac{\partial \varrho}{\partial t} + \nabla \cdot (\varrho \mathbf{V}) = 0\,, \tag{70}$$
$$\varrho \frac{\partial \mathbf{V}}{\partial t} + \varrho\,(\mathbf{V} \cdot \nabla)\,\mathbf{V} = -\nabla p + \varrho \mathbf{g} + \frac{1}{\mu}(\nabla \times \mathbf{B}) \times \mathbf{B}\,, \tag{71}$$

$$\frac{\partial p}{\partial t} + \vec{V} \cdot \nabla p = -\gamma p \nabla \cdot \vec{V} + (\gamma - 1)\nabla \cdot (\kappa \nabla T)\,, \tag{72}$$

$$\frac{\partial \mathbf{B}}{\partial t} = \nabla \times (\mathbf{V} \times \mathbf{B})\ , \tag{73}$$

$$\nabla \cdot \mathbf{B} = 0\ , \tag{74}$$

$$p = \frac{k_B}{m} \varrho T\ . \tag{75}$$

Here the unknown plasma quantities are: ϱ which is the mass density, $\mathbf{V} = [V_x, V_y, 0]$ the flow velocity, p the gas pressure, and $\mathbf{B} = [B_x, B_y, 0]$ the magnetic field. The symbol T denotes plasma temperature, $\mathbf{g} = [0, -g, 0]$ is a constant gravity, $\kappa = \kappa_0 T^{5/2}$ W m^{-1} ^{o}C^{-1} a coefficient of thermal conductivity (assumed isotropic here), $\gamma = 5/3$ is the adiabatic index, μ the magnetic permeability, k_B Boltzmann's constant and m is mean mass.

5.1.1. Thermal mode

Before presenting numerical results, we review briefly some properties of the thermal mode. We follow Field (1965) and consider a uniform, gravity-free, one-dimensional medium. A plane wave, given by $\exp[I(kx - \omega t)]$, with its cyclic frequency ω and wavenumber k is described by a dispersion relation

$$\omega^3 + I\epsilon k^2 \omega^2 - \gamma k^2 \omega - I\epsilon k^4 = 0\,, \tag{76}$$

where $I = \sqrt{-1}$, $\epsilon = (\gamma - 1)\bar{\kappa}$ and the normalized coefficient of thermal conduction,

$$\bar{\kappa} \equiv \frac{t_0 T_0}{p_0 r_0}\,. \tag{77}$$

Here the subscript $_0$ denotes a normalized quantity. We set $t_0 = 1$ s, $T_0 = 1.5$ MK is a coronal temperature, $p_0 = 10^{-2}$ Pa is a coronal gas pressure and $r_0 = 1$ Mm is a unit length. This relation is quartic in k and cubic in ω. See also De Moortel and Hood (2003) and Macnamara and Roberts (2010). There are three solutions of this dispersion relation. Two of them correspond to damped counter-propagating acoustic waves and one is a purely imaginary ω which is associated with the thermal mode. As a result, this mode does not propagate but its amplitude decays in time. For the ideal plasma of $\kappa = 0$ this imaginary ω disappears, giving a solution of $\omega = 0$.

5.1.2. Initial setup

We detail here the initial (at $t = 0$ s) setup used in our numerical simulations. In this setup the solar corona is modeled as a low mass density, highly magnetized plasma overlaying a dense photosphere/chromosphere.

The structure of the solar corona

We assume that the solar atmosphere is settled in a two-dimensional and still ($\mathbf{V}_e = 0$) environment in which the pressure gradient force is balanced by the gravity, that is

$$-\nabla p_e + \varrho_e \mathbf{g} = 0\,. \tag{78}$$

Here the subscript $_e$ corresponds to a background quantity which depends on y only. The x-component of this equation is identically zero. As gravity is pointing into the negative side of the y-axis, that is $\mathbf{g} = [0, -g, 0]$, the y-component of Eq. (78) leads to

$$-\frac{\partial p_e}{\partial y} - \varrho_e g = 0\,. \tag{79}$$

With the use of the ideal gas law, given by new (75), and the assumption of the isothermal atmosphere, $T = const$, from (79) we express background gas pressure and mass density as

$$p_e(y) = p_0 \exp\left(-\frac{y - y_\mathrm{r}}{\Lambda}\right)\,, \quad \varrho_e(y) = \frac{p_e(y)}{g\Lambda}\,. \tag{80}$$

Here $\Lambda = k_B T/(mg) = const$ is the pressure scale-height, and p_0 denotes the gas pressure at the reference level that is chosen at $y_\mathrm{r} = 10$ Mm. >From (80) we infer that $\varrho_e(y)$ falls off exponentially with height. Background mass density $\varrho_e(y)$ profile that results from (80) is displayed in Fig. 4.

As a result of (78) it follows from momentum Eq. (71) that magnetic field is force-free

$$\frac{1}{\mu}(\nabla \times \mathbf{B}_e) \times \mathbf{B}_e = 0\,. \tag{81}$$

We assume a current-free magnetic field $\nabla \times \mathbf{B_e} = 0$ such that

$$\mathbf{B_e} = \nabla \times (A\hat{\mathbf{z}})\,. \tag{82}$$

Here $\hat{\mathbf{z}}$ is a unit vector along the z-direction and A is the magnetic flux function chosen as (McLaughlin et al., 2011)

$$A(x,y) = B_0 \left[\frac{y - y_d}{(x + x_d)^2 + (y - y_d)^2} + \frac{y - y_d}{(x - x_d)^2 + (y - y_d)^2}\right]\,, \tag{83}$$

with B_0 denoting the magnetic field at the reference level $y = y_\mathrm{r} = 10$ Mm and $(\pm x_d, y_d)$ corresponding to coordinates of two dipoles. We choose and hold fixed $x_d = 10$ Mm, $y_d = 5$ Mm, and B_0 is set such that at the point $x = 0$ Mm, $y = y_\mathrm{r}$ the Alfvén speed, $c_\mathrm{A}(y_\mathrm{r}) = |\mathbf{B}_\mathrm{e}|/\sqrt{\mu\varrho_\mathrm{e}(y_\mathrm{r})}$, is ten times larger than the sound speed, $c_\mathrm{s}(y_\mathrm{r}) = \sqrt{\gamma p_\mathrm{e}(y_\mathrm{r})/\varrho_\mathrm{e}(y_\mathrm{r})}$.

Magnetic field vectors are illustrated by arrows in Fig. 4. Note that the x-point is located within the simulation region at $x = 0$ Mm and $y = 15$ Mm.

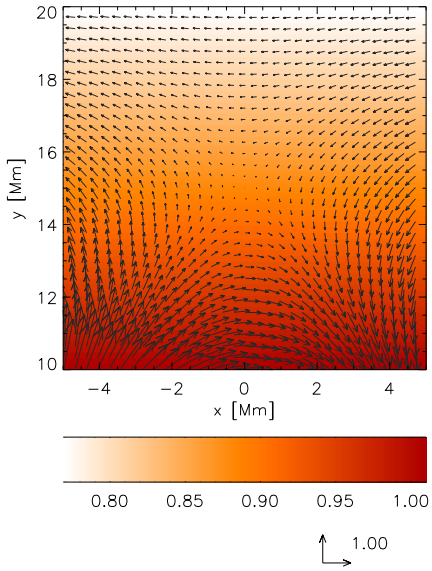

Figure 4. A background mass density (color map) and magnetic field vectors.

Initial pressure pulse

We aim to study impulsively excited thermal mode within the x-point configuration. This mode is triggered by initial pulse in gas pressure, that is

$$p(x, y, t = 0) = p_e \left[1 + A_p \exp\left(-\frac{x^2 + (y - y_0)^2}{w^2} \right) \right] . \tag{84}$$

Here A_p denotes amplitude of the initial pulse, w is its width and y_0 its vertical location. We choose and hold fixed $y_0 = 15$ Mm and so we launch the initial pulse at the x-point.

It is noteworthy here that the thermal mode was already observed in a number of circumstances. For instance, Mędrek et al. (2000) simulated sunquakes by pressure pulses. They observed that the thermal mode leads to remnants of the initial pulse, well seen in the mass density profiles at the launching place. The thermal model cannot be excited by velocity pulses and a presence of gravity is not essential for excitation of this mode as it can be launched in any uniform, gravity- and magnetic-free fluid medium (not shown).

5.2. Numerical results

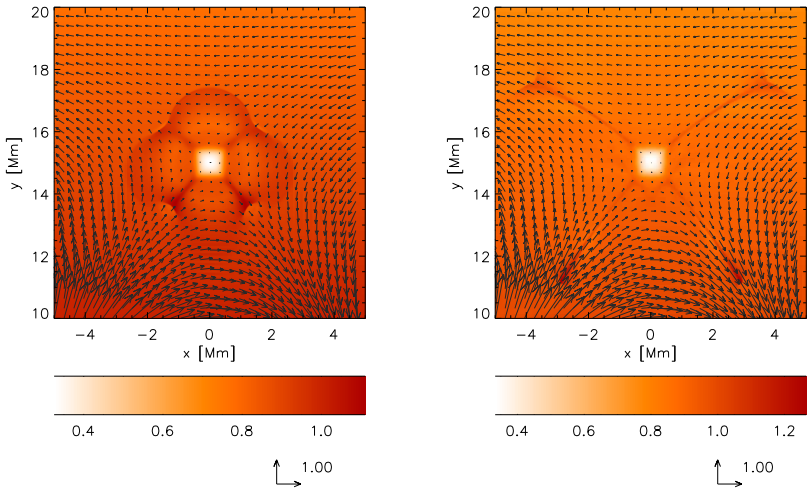

Figure 5. Mass density profiles (color maps) and magnetic field vectors at $t = 10$ s (left panel), and $t = 30$ s (right panel) for the normalized thermal conduction coefficient, $\bar{\kappa} = 10^{-4}$.

Equations (70)-(74) are solved numerically using the code *FLASH* (Fryxell et al., 2000; Lee and Deane, 2009). This code implements a second-order unsplit Godunov solver with various slope limiters and Riemann solvers as well as Adaptive Mesh Refinement (AMR) which is adopted in *Paramesh* package (MacNeice et al., 2000). We use the MUSCL-Hancock method, supplemented by the minmod slope limiter, and the Roe Riemann solver. We set the simulation box as $(-5\,\mathrm{Mm}, 5\,\mathrm{Mm}) \times (10\,\mathrm{Mm}, 20\,\mathrm{Mm})$ and time $0 \leq t \leq 2000$ s. All temporal derivatives are treated within the frame of the MUSCL-Hancock method, introduced in Section 4.1. We impose fixed in time boundary conditions for all plasma quantities in the x- and y-directions, while all plasma quantities remain invariant along the z-direction. In our studies we use AMR staggered grid (Lee and Dean, 2009) with a minimum (maximum) level of refinement set to 4 (7). The refinement strategy is based on controlling numerical errors in mass density. This results in an excellent resolution of steep spatial profiles and greatly reduces numerical diffusion at these locations. The test runs we performed for different spatial resolutions revealed a high efficiency and the convergence of the implied algorithms of the FLASH code.

As a pulse in a gas pressure warms locally plasma at the x-point this pulse

may model post-flare event (Aschwanden and Alexander, 2001). Flare models usually assume that energy is stored in the solar corona over hours or days. After this energy storage phase the onset of the flare takes place, which is associated with a sudden (over the period of 30 minutes or so), energy release. Such a strong pulse pushes out plasma, leading to rarefied region at the x-point. In the case of the ideal plasma this rarefication persists in time and the plasma remains warm at the x-point (not shown). The scenario becomes similar when the thermal conduction is switched on. However, now thermal conduction transfers energy from a hotter region to a cooler region. As a result of that, the plasma rarefication smoothes out in time. We will discuss this process below.

The pulse of Eq. (84) triggers fast and slow magnetoacoustic waves. Fast waves propagate quasi-isotropically out of the x-point, while slow waves are guided along magnetic field lines. Fast waves are well illustrated in Fig. 5 in the left panel, while slow waves are displayed in the right panel. The thermal mode is represented by mass density depression at the x-point.

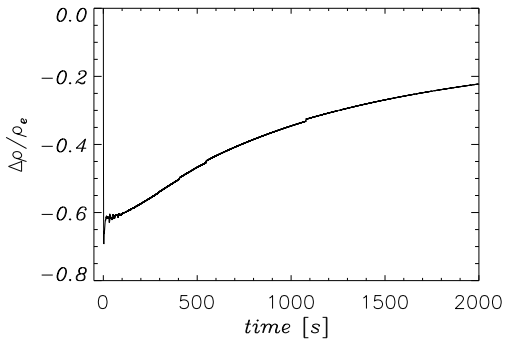

Figure 6. A typical time-signature of relative mass density, collected at the x-point, for $\bar{\kappa} = 10^{-4}$.

Fig. 6 displays the time-signature which is drawn by collecting wave signals in $\Delta\varrho \equiv (\varrho_e - \varrho)/\varrho_e$ at the detection point ($x = 0$ Mm, $y = 15$ Mm) which is located just at the x-point. This time-signature reveals the initial phase at which the mass density becomes rarefied due to the action of the initial pressure pulse. This phase lasts till $t \simeq 15$ s. Later on mass density grows in time as a result of thermal conduction. According to our expectations, the growth is higher for a larger value of $\bar{\kappa}$. Indeed, Fig. 7, which illustrates a dependence of effective damping time τ upon the normalized thermal conduction coefficient $\bar{\kappa}$, confirms our expectations. The effective damping time is obtained by assuming that $-\Delta\varrho$ decays exponentially in time as $\exp[-(t - t^*)/\tau]$. Here t^* is time

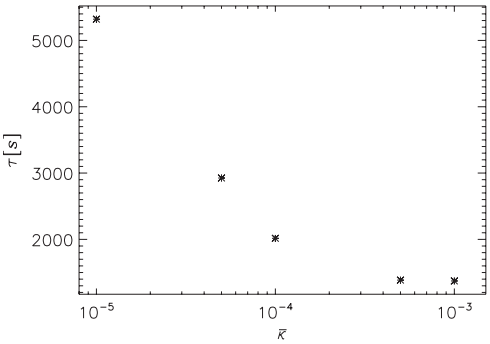

Figure 7. Plot of effective damping time τ vs. normalized thermal conduction coefficient $\bar{\kappa}$.

at which damping starts to be significant. We set $t^* = 500$ s, which is much larger than the approximate end of the initial expansion phase, 15 s. A larger (smaller) value of τ corresponds to a weaker (stronger) damping due to thermal conduction. According to our expectation τ falls off with $\bar{\kappa}$.

5.3. Summary of the numerical results

We developed a two-dimensional model of a coronal plasma to explore excitation and attenuation of the thermal mode at the x-point. We took into account constant gravity and thermal conduction. Our findings can be summarized as follows. The thermal mode can be excited impulsively by a localized pulse in gas pressure. This mode is attenuated by thermal conduction on a time-scale which depends on thermal conduction coefficient κ. For a larger value of κ this time-scale is shorter than for a smaller value. For a typical coronal value of κ this scale is 2000 s. Thus we have shown that a simple conceivable model of the solar plasma gives acceptable results, with damping times that are in good agreement with the observational data which corresponds to life-times of solar flares (Aschwanden and Alexander, 2001).

Acknowledgements

The authors express their thanks to the unknown referees for their stimulating comments. The software used in this work was in part developed by the DOE-supported ASC/Alliance Center for Astrophysical Thermonuclear Flashes at the University of Chicago. This work has been supported by a Marie Curie International Research Staff Exchange Scheme Fellowship within the 7th European Community Framework Program (K.M.). This research was carried out with the support of the "HPC Infrastructure for Grand Challenges of Science and Engineering" Project, co-financed by the European Regional Development Fund under the Innovative Economy Operational Programme (K.M.).

References

Aschwanden, M.J. and Alexander, D. (2001) Flare Plasma Cooling from 30 MK down to 1 MK modeled from Yohkoh, GOES, and TRACE observations during the Bastille Day Event (14 July 2000). *Solar Physics* **204** (1/2), 91-120.

Brackbill, J.U. and Barnes, D.C. (1980) The effect of nonzero product of magnetic gradient and B on the numerical solution of the magnetohydrodynamic equations. *J. Comp. Phys.* **35**, 426-430.

De Moortel, I. and Hood, A.W. (2003) The damping of slow MHD waves in solar coronal magnetic fields. *Astronomy and Astrophysics* **408**, 755-765.

Field, G.B. (1965) Thermal Instability. *Astrophysical Journal* **142**, 531-567.

Fryxell, B., Olson, K., Ricker, P., Timmes, F.X., Zingale, M., Truran, J.W., Lamb, D.Q., MacNeice, P., Rosner, R., and Tufo, H. (2000) FLASH: An Adaptive Mesh Hydrodynamics Code for Modeling Astrophysical Thermonuclear Flashes. *The Astrophysical Journal Supplement Series* **131** (1), 273-334.

Godunov, S.K. (1959) A difference scheme for numerical solution of discontinuous solution of hydrodynamic equations. *Math. Sb.* **47**, 271-306.

Kolgan, V.P. (1972) Application of the minimum-derivative principle in the construction of finite-diverence schemes for numerical analysis of discontinuous solutions in gas dynamics. *Uch. Zap. TsaGI* **3** (6), 68-77.

Lee, D. and Deane, A.E. (2009) An unsplit staggered mesh scheme for multidimensional magnetohydrodynamics. *J. Comput. Phys.* **228** (4), 952-975.

LeVeque, R.J. (2002) *Finite-Volume Methods for Hyperbolic Problems.* Cambridge University Press, Cambridge.

McLaughlin, J.A., Hood, A.W. and De Moortel, I. (2011) MHD Wave Propagation Near Coronal Null Points of Magnetic Fields. *Space Science Reviews* **158** (2-4), 205-236.

Macnamara, C.K. and Roberts, B. (2010) Effects of thermal conduction and compressive viscosity on the period ratio of the slow mode. *Astronomy and Astrophysics* **515**, 41-48.

MacNeice, P., Olson, K.M., Mobarry, C., de Fainchtein, R. and Packer, C. (2000) PARAMESH: A parallel adaptive mesh refinement community toolkit. *Computer Physics Communications* **126** (3), 330-354.

Mędrek, M., Murawski, K. and Nakariakov, V.M. (2000) Propagational Aspects of Sunquake Waves. *Acta Astronomica* **50**, 405-416.

Murawski, K. (2002) *Analytical and Numerical Methods for Wave Propagation in Fluids.* World Scientific, Singapore.

Murawski, K. and Lee, D. (2011) Numerical methods of solving equations of hydrodynamics from perspectives of the code FLASH. *Bull. the Polish Academy of Sc.* **59**, 81-92.

Powell, K.G. (1994) Approximate Riemann solver for magnetohydrodynamics (that works in more than one dimension). *ICASE Report No.* 94-24, Langley, VA.

Roe, P.L. (1981) Approximate Riemann solvers, parameter vectors and difference schemes. *J. Comp. Phys.* **43**, 357-372.

Toro, E. (2009) *Riemann Solvers and Numerical Methods for Fluid Dynamics.* Springer, Berlin.

van Leer, B. (1979) Towards the ultimate conservative difference scheme. V - A second-order sequel to Godunov method. *J. Comp. Phys.* **32**, 101-136.

von Neumann, J. and Richtmeyer, R.D. (1950) A method for the numerical calculation of hydrodynamic shocks. *J. Appl. Phys.* **21**, 232-237.